Highly efficient removal of arsenic metal ions with high superficial area hollow magnetite nanoparticles synthetized by AACVD method

B. Monárrez-Cordero, P. Amézaga-Madrid, W.Antúnez-Flores, C. Leyva-Porras, P. Pizá-Ruíz

Abstract

New nanotechnology alternatives and methodologies have been developed in order to overcome the limitations of conventional techniques for metal ions removal from water. Currently, the removal of heavy metals requires multiple steps which include the separation and post-treatment of the generated sludge. Usually, this sludge is composed of dangerous environmental pollutants mixed with the material used for removing the metal ion. Thus, the removal of these metals becomes a challenging task. Herein we report the synthesis of magnetite nanoparticles with high specific area by the aerosol assisted chemical vapour deposition method. Deposition temperature were fixed at 450 °C and a mixture of Ar–air were used as a carrier gas, a flow of 1.0 and 0.015 L min^{-1} were used for Ar and air, respectively. The precursor solution was a dilution of Fe (II) chloride in methanol, with different concentration 0.01, 0.05 and 0.1 mol dm^{-3}. The crystalline structure of the nanoparticles was characterized by grazing incidence X-ray diffraction. Morphology and microstructure were analyzed by field emission scanning electron microscopy, scanning probe microscopy and transmission electron microscopy. Magnetic properties were evaluated with a vibrating sample magnetometer and specific area was measured by the Brunauer–Emmett–Teller

method. To determine the removal efficiency of arsenic ion from water, several tests were carried out at six exposition times 1, 3, 5, 10, 20 and 30 min. Results showed high removal efficiency, more than 99%, in less than 1 min.

Keywords: MNPs, Nanoparticles, AACVD, Magnetite.

Introduction

In recent years, extensive work has been focused on the development of adsorbents for improving the removal of toxic heavy metal ions from wastewater. Considering the limitations of conventional methods for metal ions removal, nowadays nanotechnology is one of the most promising alternatives using magnetic nanoparticles (MNPs). MNPs are being widely studied for their characteristics of porosity, paramagnetism, crystallinity, size and high surface area. In particular, magnetite has been used as ferro- fluid [1], data storage [2], biomedicine and controlled drug delivery [3,4]. In one hand, size and morphology of the MNPs are the two main features influencing their electrical, optical and magnetic properties [5,6]. On the other hand, the synthesis method may determine their morphological structure and particle size [7–9]. Nowadays, mesoporous MNPs are an important class of new nanomaterials, which occupy an important position in materials science [10–13]. Recently, there has been a growing interest towards the use of MNPs for adsorptive removal of a variety of contaminants including organic dyes from wastewater. Owing to their several advantages over bulk magnetite particularly with respect to higher adsorption capacity, less time for reaching the adsorption equilibrium and easy magnetic separation of solids after adsorption [14–16], these MNPs also have been used as adsorbents to remove

heavy metal cations from water. The reported removal efficiency is in the range of 70–90% [17,18]. These nanoparticles are developed mainly by three different methodologies: chemical, physical and biological [13,18–21]. In any of these methods high quality materials are obtained. Anyhow, one of the main disadvantages in the chemical method is the requirement of multiple steps during the synthesis. Physical methodologies have a key drawback, they are expensive and require demanding infrastructure such are high vacuum equipment, precise gas control, etc. However, there are economic and achievable techniques by which it is feasible to synthesis nanoparticles with high surface area. Aerosol assisted chemical vapour deposition (AACVD) is a variant of chemical vapour deposition technique, it is an attractive method for the preparation of nanoparticles of different materials with good characteristics and high quality [22–25]. In AACVD, the structural morphology of resultant nanoparticles strongly depends on the precursors and operating conditions. Some advantages of this technique are the fast production rate, continuous operation, the use of relatively simple equipment and the possibility to scale the process industrially. Here, we report the synthesis of hollow magnetite nanoparticles by the AACVD method; there are scarce reports on the synthesis of hollow iron oxide nanoparticles by this technique. Microstructural characterization was realized by grazing incidence X-ray diffraction, field emission scanning and transmission electron microscopy. Surface area was measured with Brunauer–Emmett–Teller (BET) method. Arsenic removal tests were realized at different contact times of nanoparticles-arsenic solutions. Removal efficiency was

determined by atomic absorption spectroscopy (AAS) of decanted liquid to detect arsenic and iron.

Material and methods

Synthesis of hollow iron oxide nanoparticles: MNPs were synthetized by AACVD technique. Fig. 1 shows the AACVD system used to synthesize the hollow MNPs. It mainly consists of an ultrasonic nebulizer (a), in which the precursor solution (b) is converted into a fine aerosol. The starting solution was a dilution of Fe (II) chloride in methanol (99.9%), three different concentrations, 0.01, 0.05 and 0.1 mol dm^{-3}, were tried. The aerosol was carried by a mixture of Ar–air flow, of 1.0 and 0.015 L min^{-1}, respectively. Then, the volumetric air/Ar ratio was 0.015. Ar gas was employed to avoid excessive oxidation of the iron precursor. The aerosol was injected into a vycor tube (c), which takes place as a reaction chamber (d). The tube was located inside a cylindrical furnace (e), which has a very precise temperature control (±1 °C). Synthesis temperature was fixed at 450 °C. This temperature was selected since thermogravimetric analysis results of the precursor salt showed that Fe chloride decomposition and formation of iron oxide starts around 420 °C. Finally, at the outermost side of vycor tube it is connected a right angle nozzle (f) which is introduced into a flask with methanol (g) to collect the nanoparticles. The collection flask is placed on super magnets which have the function to attract and concentrate the MNPs obtained.

MNPs characterization: electron microscopy (SEM) in a JEOL JSM-7401F and by a high resolution transmission electron microscope (HRTEM) in a JEOL JEM-2200FS.

In addition, elemental analysis of the MNPs was achieved by means of energy dispersive X-ray spectroscopy (EDS) in a Oxford Inca microanalysis system. Crystalline structure was analyzed by grazing incidence X-ray diffraction (GIXRD) in a Panalytical X-Pert system; the patterns were obtained using Cu Kα radiation at 40 kV and 35 mA. Diffracted beam path included a graphite flat crystal monochromator. Grazing incidence angle was fixed at 0.5°; whereas the scanning angle 2θ was varied between 25° and 80°, at 0.02 and 12 s for step size and step time, respectively. From these analyses, nanoparticles composition, morphology, particle size and crystalline structure were studied as a function of the preparation conditions. A vibrating-sample magnetometer was used to study the magnetic properties of magnetite hollow nanoparticles. Specific surface area determination was measured by the BET method.

Arsenic removal tests: Sodium (meta)arsenite ($NaAsO_2$) and sodium arsenate heptahydrate ($Na_2HAsO_4 \cdot 7H_2O$) were dissolved separately in distilled water (99% purity, JT Baker) to obtain stock solutions of As^{+3} and As^{+5} at 0.05 and 0.08 ppm, respectively.

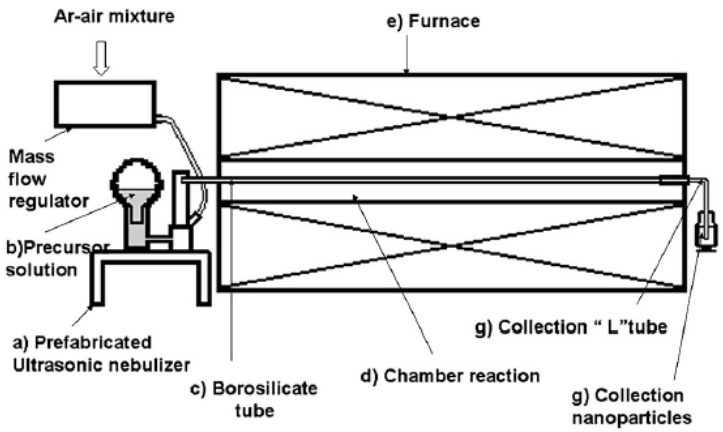

Fig. 1. Schematic diagram of AACVD system utilized to prepare MNPs.

Contact tests between arsenic ions and iron oxide nanoparticles were done at room temperature. In order to determine the arsenic adsorption kinetics, 10 mg of nanoparticles were added to each arsenic solution (As^{+3} or As^{+5}) and thoroughly mixed with a mechanical stirrer during different times 1, 3, 5 10, 20 and 30 min. After the mixing time, the nanoparticles were recovered by placing a magnet inside the beaker.

Nanoparticles were fully attracted by the magnet and the solution became clear. The content of both, iron and arsenic in the remaining solution was further quantified by atomic absorption spectroscopy using AAS GBC, model Avanta Sigma. This examination was repeated twice in order to test the reproducibility of our experiments.

Finally, with the aim of observing the arsenic trapped on the metal nanoparticles, the nanoparticles were mixed with a 500 ppm arsenic solution by 1 min. After recovering and drying the nanoparticles, these were analyzed by SEM.

Results and discussion

Microstructure of MNPs: Uniform hollow MNPs were successfully synthesized by AACVD technique. SEM images showed an average size of 200 nm, with typical spherical morphology, which tend to agglomerate. It is interesting to note that these nanoparticles are hollow and have a high porosity, advantageous properties for metal removal property. It is proposed that the combined effect of droplet size, precursor solution concentration, residence time, temperature distribution in the reaction chamber and the heating rate of droplet/particle determine the growth and microstructure on the synthesized nanoparticles. The formation of hollow particles can be related to the localized super-saturation of the solute with the consequent formation of a crust on the

droplets surface [22]; which depends on the evaporation rate of the solvent, and on the strength and permeability of the crust. For high residence time and precursor solution concentration the crust is formed earlier on the droplet surface, given rise after complete evaporation of solvent to hollow particles, these results coincides with previous reports [21–25]. Additionally, hollow nanoparticles can break into irregular and small particles as it is shown in electron microscopy micrographs.

Fig. 2 shows secondary electron SEM micrographs of hollow MNPs obtained at different precursor solution concentration. It was observed that at concentration of 0.01 mol dm^{-3} (Fig. 2a) finer nanoparticles were obtained, consisting of hollow structure of one or several crystallite layers. Increasing the concentration to 0.05 and 0.1 mol dm^{-3} (Fig. 2b and c) MNPs average diameter increases, although hollow structure is conserved. These results were confirmed by HRTEM analysis. The elemental composition of the nanoparticles was studied by EDS; any contamination was detected, in particular none appreciable residue of chlorine. Results showed that the atomic ratio Fe/O is very close to the stoichiometric concentration. These results indicate that the synthesis was performed uniformly, resulting in clean nanoparticles; and the process was successfully optimized, since a tight stoichiometry was reached. Thus, unlike other techniques where a further cleaning process is necessary in order to remove the unreacted material [13,26–27], AACVD is a suitable one-step technique, for synthetizing high quality magnetite nanoparticles.

The effect of both, the concentration of the solution precursor and the flow of the carrier gas was analyzed by HRTEM. Fig. 3a shows a bright field TEM image of MNPs

synthesized with a solution of 0.01 mol dm^{-3}; the average sphere size was around of 200 nm. The nanoparticles were well defined spheres and the crystallite size was between 5 and 20 nm. When the concentration was increased five times to 0.05 mol dm^{-3}, (see Fig. 3b) the average particle and the crystallite size remains the same; however, the surface of the nanoparticle seems to be denser and the thickness of the crust layer larger. Now, when the concentration was increased to 0.1 mol dm^{-3}, (see Fig. 3c) the average particle size increased to 2050nm. Also the thickness of the crust layer increased, observing multilayers.

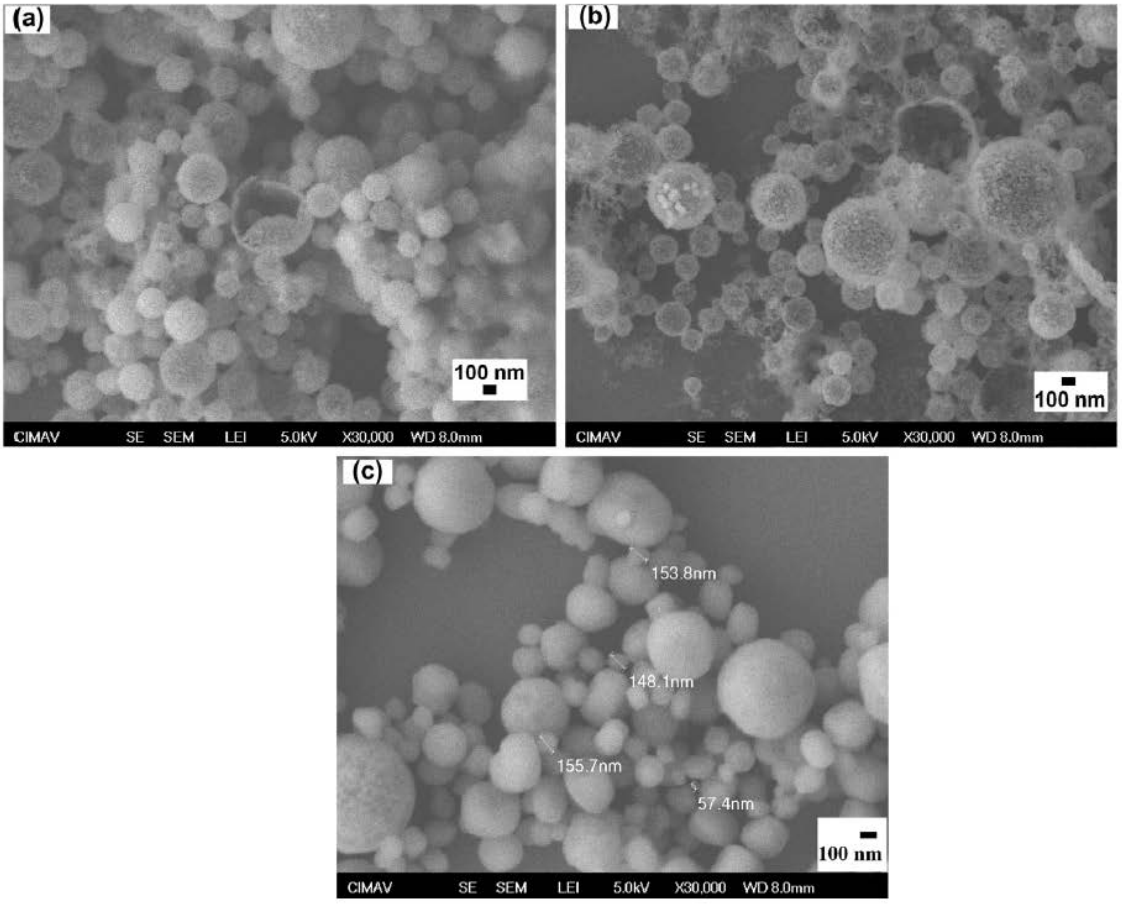

Fig. 2. SEM images of the MNPs, (a) at 0.01 M; (b) at 0.05 M; and (c) at 0.1 M, the three concentration was at 450 °C with an Ar–air mixture flow of 1 L min^{-1} and 0.015 L min^{-1} respectively.

The crystallite size increased to a size larger than 30 nm. Anyhow, the three concentrations tested produced hollow nanoparticles and the overall effect of varying the concentration of the precursor is clearly observed in the thickness of the crust layer of the nanoparticle and in the size of the crystallite. This trend is due to a rapid evaporation of the solvent and having a surface precipitation of the salt, it can be said that one has a locally supersaturated solution, thus diffusion of species is slow compared to the rate of evaporation of the solvent [28].

Fig. 4 shows XRD patterns for polycrystalline magnetite nanoparticles synthesized at different concentrations. It can be observed the representative peaks corresponding to principally the magnetite (Fe_3O_4) phase [29], small quantities of Fe_2O_3 were detected. The strong and sharp peaks confirmed that the samples are well crystallized phase. The peaks that are not indexed belong to the silicon substrate. The average size of the crystallites that are present in the shell of the nanoparticles was estimated from peak broadening of X-ray diffraction pattern, we found around 15– 20 nm. The crystallite size is very similar to those obtained by other authors [30–31]. However, the crystallite size obtained experimentally in this work was considerably smaller than those calculated from the average droplet size and solution concentration. The diameter of the particle can be estimated considering that the entire precursor contained in one droplet produce only one particle, and a droplet size of 2.3 μm [32]. We found 267 nm for the highest concentration (0.1 mol dm^{-3}) and 124 nm for the solution of 0.01 mol dm^{-3}. These values are comparable to the highest diameters of the hollow particles observed in SEM analysis. In addition, the quantity of crystallites

produced by the precursor contained in one droplet was calculated. Considering crystallites of 15 nm of diameter, one droplet of 0.01 solution generate more than 560 crystallites. Table 1 resumes the results of this estimation.

Magnetic and surface area measurements: Fig. 5 shows the magnetization curve for the MNPs, it is shown a typical curve of a super paramagnetic material, which has a specific saturation magnetization (Ms) of 43 emu g^{-1}, with a remnant magnetization (Mr) of almost zero, characteristics of magnetically soft material allowing them to be easily demagnetized. This information helps to know that the hollow structures exhibit a paramagnetic at ambient temperature. It is known according to work performed by Huang et al. [13] that higher magnetic parameters of the structures is related with higher crystallinity and higher particle size. In addition, this property is an advantage for our application, because in this way the nanoparticles can be easily manipulated for precipitation and collection.

On the other hand, since adsorption capacity strongly depends on the specific surface area of the adsorbents, its value for each material is determined by BET method. The Figs. 6 and 7 show the isotherm calculated by this method and pore size distribution of the hollow nanoparticles respectively, confirming that the nanoparticles have a mesoporous structure, since the isotherm obtained was of type IV. The surface area calculated was 62.2 m^2/g, which correspond to an average particle size of 19 nm. This is consistent with results of microstructural characterization; the hollow nanoparticles, has high porosity which cause the large surface area. The pore size distribution derived from desorption data reveals a heterogeneous distribution and

presents no special behavior although there are some peaks at 2, 2.5 and 5 nm, it also has a wide peak in the range of 5–20 nm.

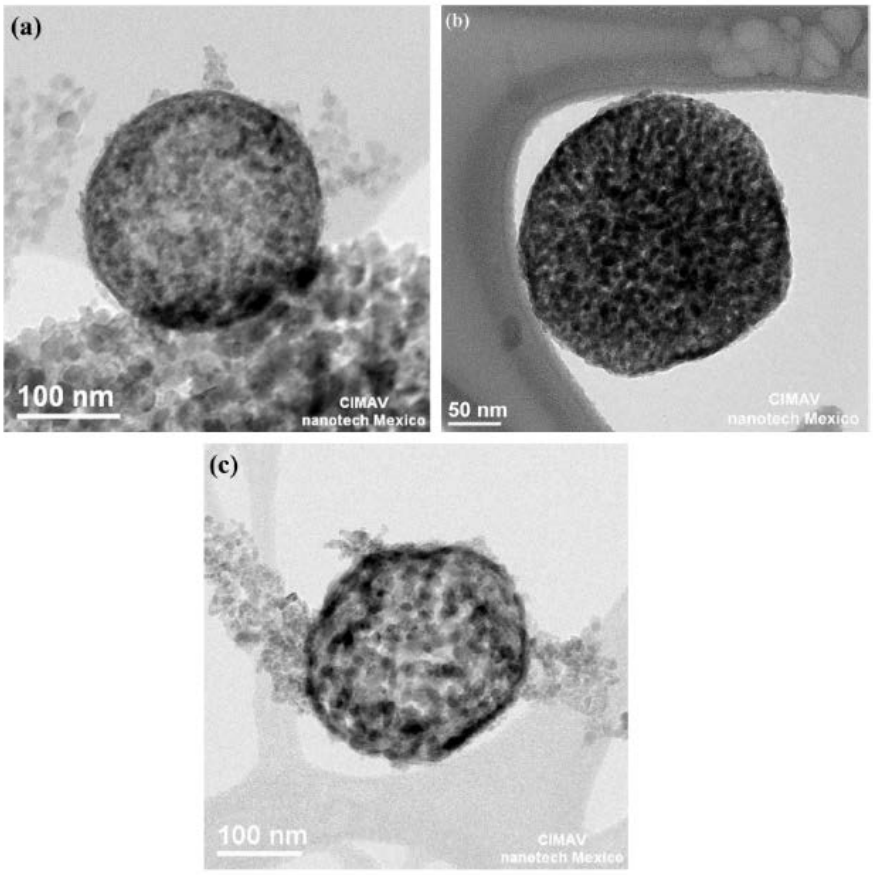

Fig. 3. TEM images of the hollows MNPs, (a) at 0.01 M; (b) at 0.05 M; and (c) at 0.1 M, the three concentration was at 450 °C with an Ar–air mixture flow of 1 L min^{-1} and 0.015 L min^{-1} respectively.

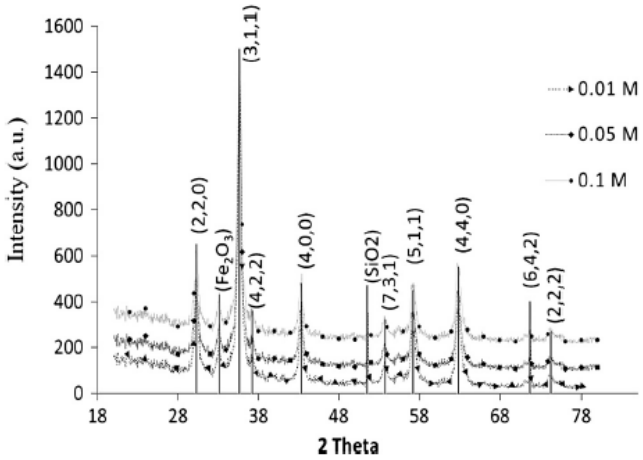

Fig. 4. Typical XRD spectra of magnetite NPs, at 0.01, 0.05 and 0.01 M.

Table 1
Estimation of average particle diameter and number of crystallites of Fe_3O_4 produced for each droplet as a function of solution concentration. Average droplet diameter 2.3 µm. Density of crystallites 5.0 g/cm^3.

Solution concentration [mol dm^{-3}]	Average particle diameter [nm]	Crystallites 15 nm	Crystallites 30 nm
0.1	267	5647	706
0.05	212	2824	353
0.01	124	565	71

Arsenic adsorption: As mentioned in the experimental section, the arsenic removal tests were repeated in order to verify the reproducibility. Results were remarkable since it was found a very high efficiency for removal of both, As^{+3} and As^{+5} ions. Before one minute of contact, arsenic ions were completely removed from water achieving almost 100% of efficiency.

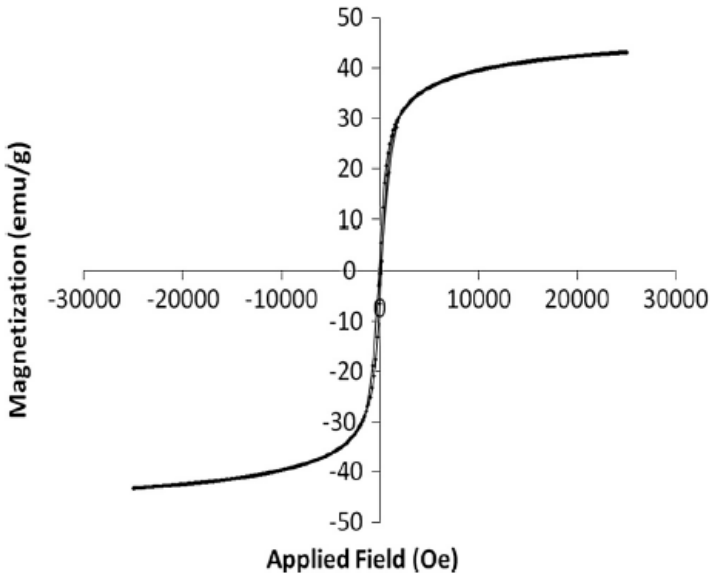

Fig. 5. Room-temperature magnetization curve of MNPs synthetized in this work.

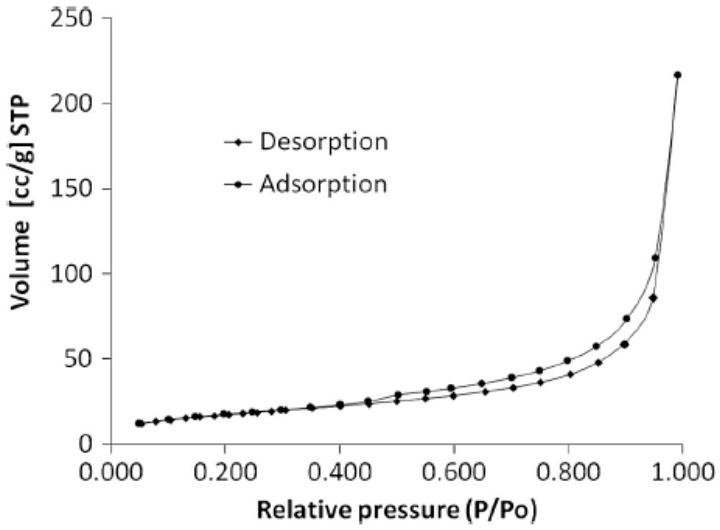

Fig. 6. Adsorption–desorption isotherm for mesoporous hollow MNPs synthetized in this work.

Thus, arsenic removal was carried out very fast, which means that the affinity of arsenic by the iron is very strong. Besides this affinity, the rapid adsorption of the metal ions on the MNPs is also produced by the high specific surface area of the adsorbents. In the literature there are other reports where arsenic is removed by iron oxide nanoparticles [18,33]. However, their results showed exposition times of nanoparticles to arsenic ion from 30 to 120 min, to achieve a removal efficiency of 85%. Then, the results presented in this work are certainly remarkable.

Furthermore, another advantage of using this type of particles in the removal or arsenic is the facility of nanoparticles recollection from the tested solution. Due to the paramagnetic nature of the particles, these are easily to separate from the tested solution with the help of super-magnets. For this reason the effluent of tested solution from each flask was analyzed. The iron content in all samples was found to be undetectable. All the MNPs were attracted by the super-magnets, achieving a

successfully separation. Then, this feature makes more attractive the use of this type of nanoparticles in the removal of heavy metal ions, since the sludge produced are easily separated from the flow of treated water.

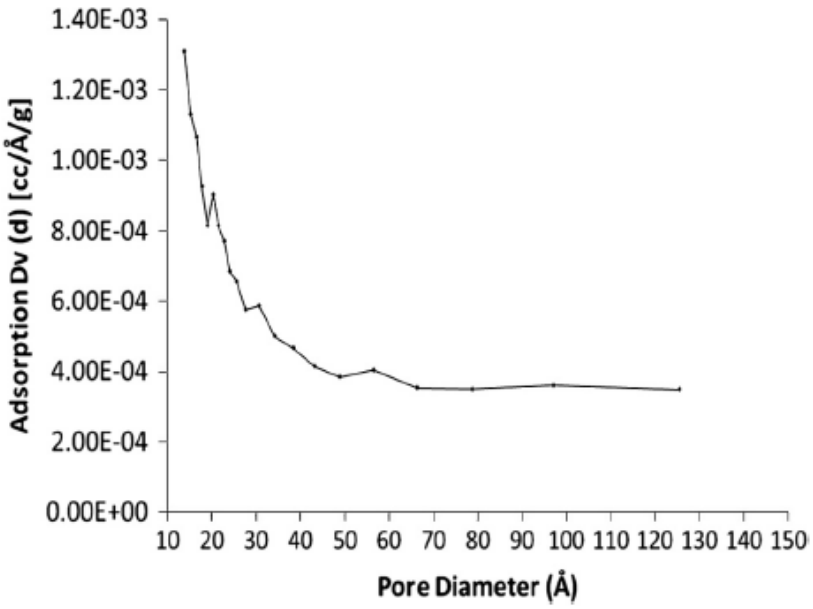

Fig. 7. The pore size distribution for the MNPs synthetized in this work.

Conclusions

High specific area iron oxide nanoparticles were obtained by aerosol assisted CVD technique. Microstructural characterization shows that magnetite phase was the principal component, only small quantity of ferrite phase was observed. Most of the nanoparticles were spherical, composed of many crystallites of 10–20 nm of size, forming a spherical shell with external diameter around 280 ± 10 nm, and thickness of about 20 ± 3 nm. Magnetization studies showed that MNPs are paramagnetic, with specific saturation magnetization of 43 emu g^{-1}. Specific area was determined around

62 m^2 g^{-1}. Very high efficiency of As ion removal in solution was obtained; complete removal in around one minute of contact of the MNPs with the solution.

Acknowledgment

The authors would like to thank E. Torres, K. Campos, C. Ornelas, O. Solis, R. Ochoa, S. Miranda, A. Rubio, D. Lardizabal for their technical assistance.

References

[1] L.J. Love, J.F. Jansen, T.E. Mcknight, Y. Roh, T.J. Phelps, L.W. Yeary, G.T. Cunningham, IEEE ASME Trans. Mecatron. 10 (2005) 68–76.

[2] A. Chakraborty, J. Magn. Magn. Mater. 204 (1999) 57–60.

[3] D.K. Kim, M. Mikhaylova, F.H. Wang, J. Kehr, B. Bjelke, Y. Zhang, T. Tsakalakos, M. Muhammed, Chem. Mater. 15 (2003) 4343–4351.

[4] A.K. Gupta, S. Wells, IEEE Trans. Nanobiosci. 3 (2004) 66–73.

[5] J.S. Bradley, B. Tesche, W. Busser, M. Masse, R.T. Reetz, J. Am. Chem. Soc. 122 (2000) 4631–4636.

[6] T. Sugimoto, Y.S. Wang, J. Colloid Interface Sci. 207 (1998) 137–149.

[7] C.N.R. Rao, G.U. KulKarni, P.J. Thomas, P.P. Edwards, Chem. Soc. Rev. 29 (2000) 27–35.

[8] X.H. Liu, G.Z. Qiu, X.G. Li, Nanotechnology 16 (2005) 3035–3040.

[9] A.L. Andrade, M.A. Valente, J.M.F. Ferreira, J.D. Fabris, J. Magn. Magn. Mater. 324 (2012) 1753–1757.

[10] X. Xin, Q. Wei, J. Yang, L. Yan, R. Feng, G. Chen, B. Du, H. Li, J. Chem. Eng. 184 (2012) 132–140.

[11] A. Mitra, C. Vázquez, M.A. López, B.K. Paul, A. Bhaumik, Micropor. Mesopor. Mater. 131 (2010) 373–377.

[12] R. El-kharrag, A. Amin, Y.E. Greish, Ceram. Int. 38 (2012) 627–634.

[13] Z. Huang, F. Tang, J. Colloid Interface Sci. 281 (2005) 432–436.

[14] M.H. Liao, D.H. Chen, J. Mater. Chem. 12 (2002) 3654–3659.

[15] Y.F. Shen, J. Tang, Z.H. Nie, Y.D. Wang, Y. Ren, L. Zuo, Sep. Purif. Technol. 68 (2009) 312–319.

[16] Y.F. Shen, J. Tang, Z.H. Nie, Y.D. Wang, Y. Ren, L. Zuo, Bioresour. Technol. 100 (2009) 4139–4146.

[17] M. Abhijit, D.G. Sunando, K.B. Jayant, D. Sirshendu, Sep. Purif. Technol. 55 (2007) 3–8.

[18] T. Tuutijärvi, J. Lub, M. Sillanpää, G. Shen, J. Hazard. Mater. 166 (2009) 1415–1420.

[19] M. Mahmoudi, S. Sant, B. Wang, S. Laurent, T. Sen, Adv. Drug Delivery Rev. 63 (2011) 24–46.

[20] B.W. Muller, R.H. Muller, J. Pharm. Sci. 73 (1984) 919–922.

[21] P. Tartaj, M.P. Morales, T. Gonzalez, S. Veintenillas, C.J. Serna, J. Magn. Magn. Mater. 290–291 (2004) 28–34.

[22] H.E. Esparza-Ponce, A. Reyes-Rojas, W. Antúnez-Flores, M. Miki-Yoshida, Mater. Sci. Eng. A343 (2003) 82–88.

[23] G.L. Messing, S. Zhang, G.V. Jayanthi, J. Am. Ceram. Soc. 76 (1993) 2707–2726.

[24] D.J. Janackovic, V. Jokanovic, L.J. Kostic-Gvozdenovic, S. Zec, J. Mater. Sci. 32 (1997) 163–168.

[25] E. Djurado, E. Meunier, J. Solid State Chem. 141 (1998) 191–198.

[26] N. Guan, J. Xu, L. Wang, D. Sun, Colloid Surf. A 346 (2009) 221–228.

[27] X. Wei, C. Roger, R.C. Viadero, Colloid Surf. A 294 (2007) 280–286.

[28] Ch. Seo-Yong, L. Jong-Heun, P. Soon Ja, J. Mater. Sci. 30 (1995) 3274–3278.

[29] Joint Committee on Powder Diffraction Standards, Powder Diffraction File, International Center for Diffraction Data, Swarthmore, PA, 2006. card 00-088-0315.

[30] K. Simeonidis, T. Gkinis, S. Tresintsi, C. Martinez, G. Vourlias, I. Tsiaoussis, G. Stavropoulos, M. Mitrakas, M. Angelakeris, Chem. Eng. J. 168 (2011) 1008–1015.

[31] R.Y. Hong, T.T. Pan, H.Z. Li, J. Magn. Magn. Mater. 303 (2006) 60–68.

[32] Measured in our laboratory by interferometry in a Masterisized 2000 system.

[33] W. Tang, Q. Li, S. Gao, J.K. Shang, J. Hazard. Mater. 192 (2011) 131–138.